DRIVE
Drought Resilience Improvement in Vineyard Ecosystems

LIFE19 ENV/IT/000035

Report on vineyard water deficit maps in the two areas and list of DEMO farms components

Sub-action A.1 "*Study of vineyard water deficit components and constitution of DEMO farmer group*"
15.04.2021

Table of contents

Introduction to the deliverable

The objectives of Sub-action A.1 "*Study of vineyard water deficit components and constitution of DEMO farmer group*" were:

- the development of models and databases for the spatially distributed simulation of water deficit in vineyards;
- the use of such products to derive vineyard water deficit maps for the study area;
- the use of the water deficit maps to identify DEMO farms where carrying out the other project activities.

Besides the current one, this document is articulated in the following sections:

- Materials and methods, in which the development of the weather and soil databses, and of the modelling solutions are presented in three dedicated subsections;
- Results and discussion, in which two subsections are used to present results related with the water deficit maps and with the identification of the DEMO farms;
- References.

Although its complexity and requirements in terms of computational time, the approach based on biophysical simulations to develop the water deficit maps was preferred to classical approaches based on agro-ecological indicators (e.g., Confalonieri et al., 2010a). Indeed, despite the variety of indices available in the literature that explicitly target issues related with the unbalance between rainfall and evapotranspirative demand from the atmosphere (e.g., De Martonne, 1942; Carter and Mather, 1966; Budyko, 1974; Confalonieri et al., 2010b), none of them was considered suitable for describing seasonal water deficit dynamics in peculiar system like vineyards.

Materials and methods

Spatially distributed simulations of water deficit were made possible:

- by the development of a dedicated database containing
  - weather (from 2009 to 2020) and
  - soil data, and
- by the development of a dedicated modelling solution that included models for estimating
  - reference evapotranspiration,
  - dynamic crop coefficients to derive the evapotranspiration of the vineyard (unlimited by water),
  - soil water redistribution, and
  - root water uptake.

Weather database

The weather database used for the simulations of vineyard water deficit is based on the historical European dataset of daily meteorological data of the University of Milan Cassandra Lab (Figs. 1 and 2). The database includes historical and near real time data, the latter constantly updated with a 2-day delay, and it covers the whole European area since 1 January 2000, gathering data from the international networks of NOAA-GSOD (NOAA, 2020a), METAR (NOAA, 2020b) and SYNOP (NOAA, 2020c) and from several Regional Extension and Environmental Services.
Starting from the set of weather station data, daily European layers (with an average spatial resolution of about 2 km × 2 km – 0.016° × 0.016°) of maximum and minimum temperature, precipitation, solar radiation, maximum and minimum relative humidity, wind speed and reference evapotranspiration are obtained by means of dedicated geostatistical techniques and modelling tools.
Temperature grids are obtained by means of squared inverse distance weighting (IDW), homogenized for elevation by means of monthly altitudinal gradients (Mariani et al., 2012; Mariani et al., 2016; Cola et al., 2020). The reference digital terrain elevation model adopted for data spatialization is resampled USGS Gtopo30 (USGS, 2020). Other variables are obtained with simple IDW method, whereas reference evapotranspiration is obtained from the layers of the driving atmospheric variables by means of Penman-Monteith method (Allen et al., 1998).
The dataset supports the research activities of Cassandra Lab and of Cassandra Tech s.r.l. (a spinoff supported by the University of Milan), making possible the parameterization and evaluation of several modelling tools, as well as the delivery of services, thanks to its spatial and temporal extent and resolution.
The near real time data are integrated with a forecasting system with the aim of projecting agroenvironmental simulations two weeks forward with respect to the current day. To reach this aim, the 0:00 UTC forecasts from the global GFS model

(NOAA, 2020d) are daily acquired. This infomation is integrated with available archive data by means of proprietary MOS post-processing techniques in order to correct forecasted data through the intercalibration with previous observative data. This also allows downscaling the forecasted weather data to the same spatial resolution of the archive and near real time datasets (2 km × 2 km).

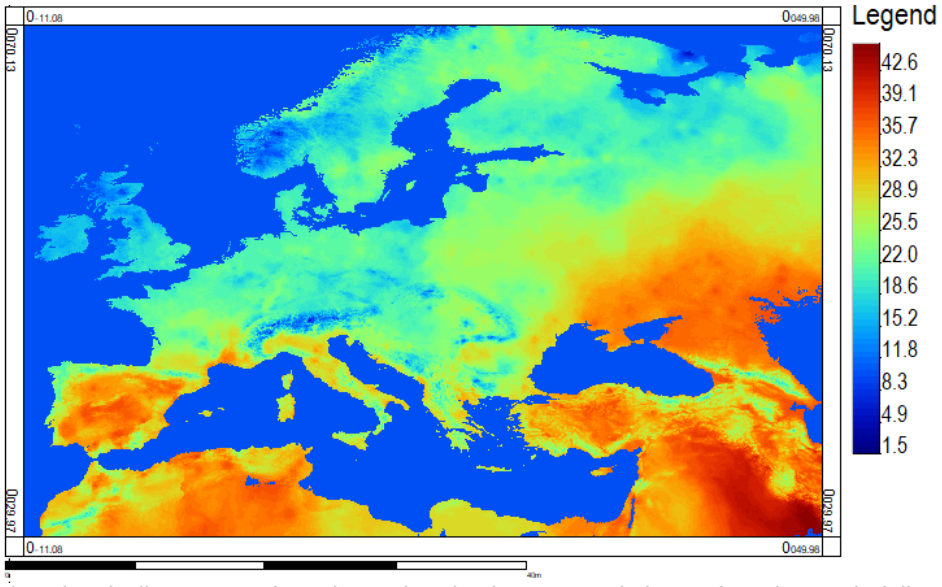

Figure 1. University of Milan Cassandra Lab weather database. Sample layer of maximum air daily temperature.

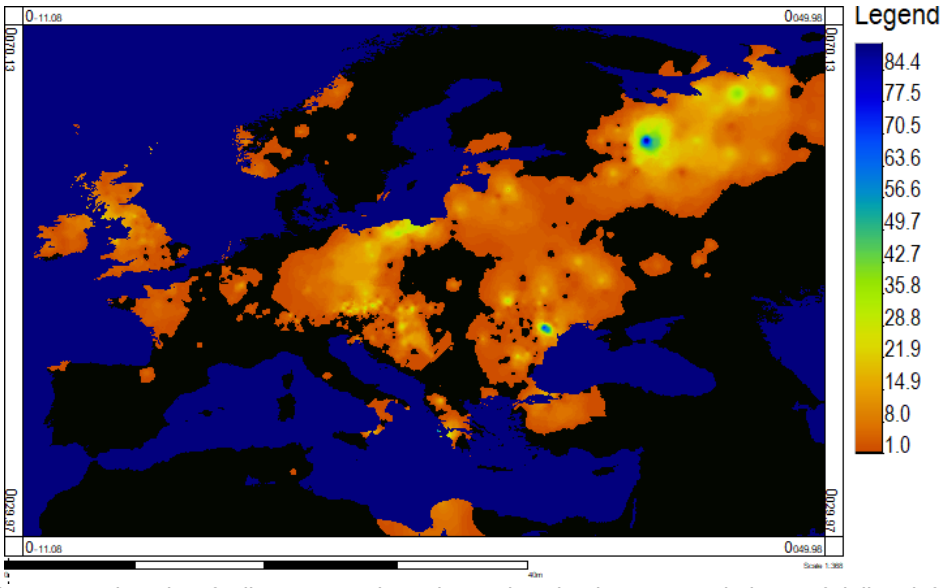

Figure 2. University of Milan Cassandra Lab weather database. Sample layer of daily rainfall.

Soil database

To get the highest consistency between the sources of information for soil physical properties in the two areas, the WISE (World Inventory of Soil Emission potentials; version WISE30sec 1.0 – 30 by 30 arc-seconds) soil database (Batjes, 2016) was used, given it was explicitly developed to provide inputs to run agro-environmental simulation models. This makes this database as particularly suitable for the purpose of zonations targeting the variable of interest (i.e., water deficit).
The WISE database is based on soil mapping units with explicit geographical coordinates (Fig. 3). A number of soil typological units are then identified for each soil mapping unit. Soil typological units do not have an explicit spatial dimension (they do not have geographical coordinates) but they are present in each soil mapping units in relative terms,

i.e., percentage presence of a given soil typological unit within a soil mapping unit (Table 1). Physical and chemical soil properties are associated to soil typological units.
This structure is shared among the main soil databases like, e.g., the European Soil Database (Panagos et al., 2012), and it requires to run a simulation for each soil typological unit (in whatever point within a soil mapping unit) and to aggregate simulation results by making the mean of the values simulated for the soil typological units weighted by the percentage of relative presence of the soil typological units within the soil mapping unit.
Soil texture percentage sand, silt, clay, organic carbon, skeleton and bulk density data were derived from the WISE database and pedotransfer functions (van Genuchten, 1980) were used to derive, for each soil typological unit, soil water contents at permanent wilting point and field capacity, needed to run the model for soil water redistribution (see section "*Simulation of water deficit*" in this document).

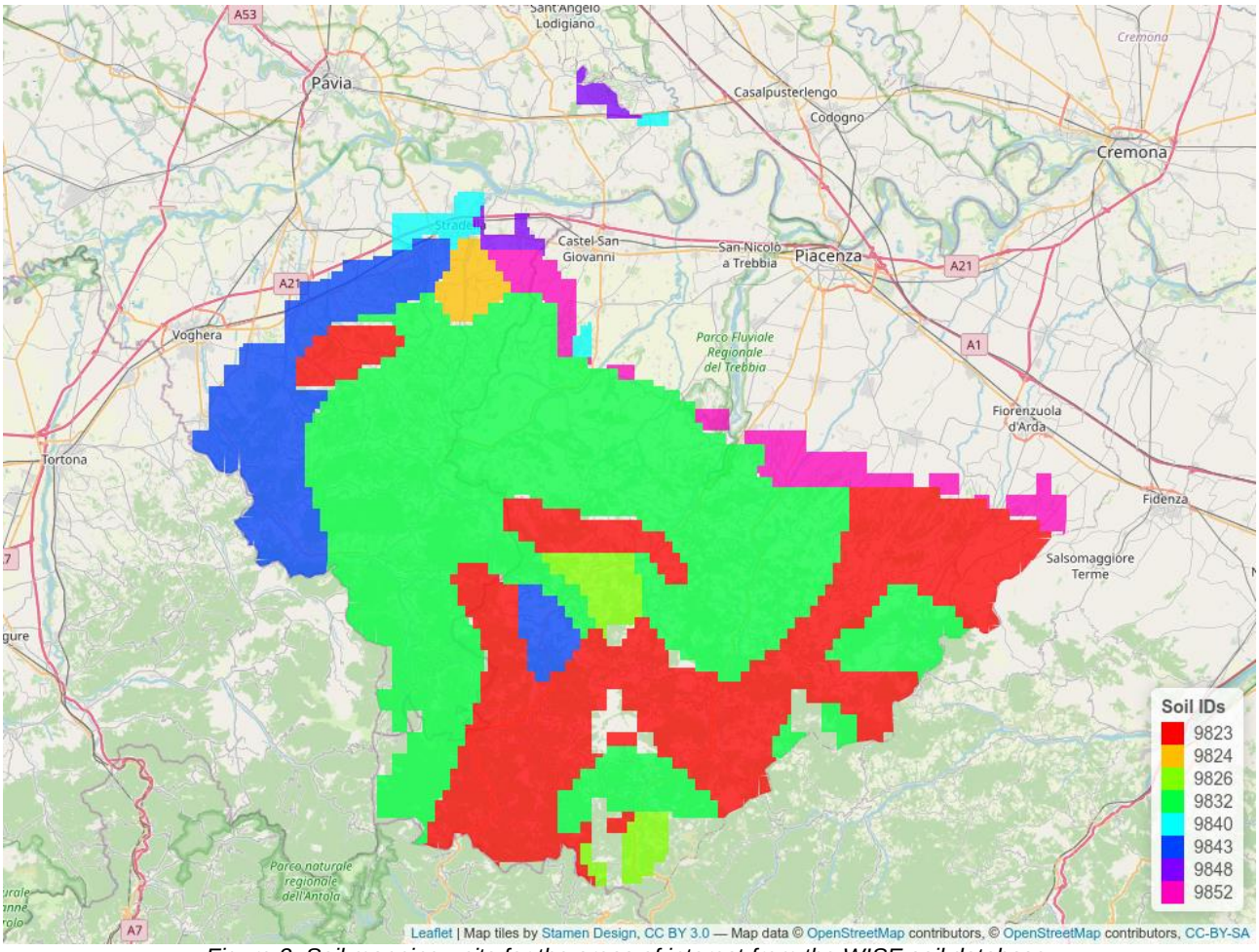

Figure 3. Soil mapping units for the areas of interest from the WISE soil database.

Table 1. Relative presence of soil typological units for each of the soil mapping units (see Figure 3) of interest for the study areas.

Soil mapping unit	Soil typological unit	Percentage presence within the soil mapping unit	Sand (%)	Clay (%)	Silt (%)	Skeleton (%)	Soil organic carbon (%)
9823	20	16.67	40.33	20.33	39.33	13.67	1.31
9823	22	5.56	29.67	20.67	49.67	2.67	1.12
9823	23	5.56	39.33	19.67	41	11	1.22
9823	24	38.89	43.33	24.33	32.33	14.67	0.79
9823	25	33.33	55.67	16.67	27.67	17.67	0.95
9824	1	14.44	30.33	29.67	40	5.33	1.04
9824	2	13.33	40.33	20.33	39.33	13.67	1.31
9824	3	22.22	16.33	48	35.67	4	1.33
9824	5	11.11	39.33	19.67	41	11	1.22
9824	6	11.11	43.33	24.33	32.33	14.67	0.79
9824	7	11.11	55.67	16.67	27.67	17.67	0.95
9824	8	16.67	12.67	56	31.33	4	1.57
9826	26	20.00	44.33	10.67	45	16	3.48
9826	27	20.00	42	14.33	43.67	23	6.15
9826	30	60.00	31	21	48	9	1.27
9832	17	60.00	40.33	20.33	39.33	13.67	1.31
9832	19	40.00	39.33	19.67	41	11	1.22
9840	31	50.00	40.33	20.33	39.33	13.67	1.31
9840	32	15.00	25.33	28.67	46	8	1.8
9840	33	30.00	36.67	21.33	42	3.33	0.92
9840	34	5.00	12.67	56	31.33	4	1.57
9843	13	55.56	43.67	20.33	36	18.33	2.17
9843	14	33.33	40.33	20.33	39.33	13.67	1.31
9843	16	11.11	39.33	19.67	41	11	1.22
9848	35	20.00	43.67	20.33	36	18.33	2.17
9848	36	30.00	40.33	20.33	39.33	13.67	1.31
9848	37	10.00	36.67	21.33	42	3.33	0.92
9848	38	40.00	39.33	19.67	41	11	1.22
9852	9	10.00	40.33	20.33	39.33	13.67	1.31
9852	10	10.00	36.67	21.33	42	3.33	0.92
9852	11	50.00	29.67	20.67	49.67	2.67	1.12
9852	12	30.00	39.33	19.67	41	11	1.22

Simulation of water deficit

According to the reference approach of the FAO paper 56 (Allen et al., 1998), grapevine maximum evapotranspiration is obtained by applying a dynamic multiplicative factor Kc to the reference crop evapotranspiration ET_0, the latter being estimated according to the Penman-Monteith model (Allen et al., 1998).
In this study, in order to overcome the simplistic approach of the FAO Paper 56 where three discontinuous values of Kc are used for the initial, full-canopy and late stages, a more physiologically-sound approach has been followed, based on Kc values dynamically derived form the phenological development stage of the grape.
In this regard, a simplified version of the Iphen phenological model for grapevine (Mariani et al., 2013, Cola et al., 2014, Cola et al., 2017) has been adopted and parameterized in order to describe the development of five different ripening classes (early, medium-early, medium, medium-late, late) on the basis of historical phenological data (Calò et al., 2017). The model translates the daily accumulation of thermal units into the corresponding vegetative and reproductive phenological stage, codified according to the BBCH reference scale for grape (Meier, 2003).
Hence, Kc has been obtained as function of the phenological stage and the consequent development of grape canopy (Cola et al. 2014), determining the fraction of intercepted incoming global solar radiation (Riou et al.,1989).

Soil water redistribution was simulated using the cascading approach (also known as tipping bucket model), which is the most widespread method to simulate vertical water movements in agricultural soils. The cascading model assumes that water can move only downward in the soil profile (Romano et al., 1998). Water movements occur when the water content in a soil layer exceeds field capacity. The water in excess is then transferred to the underlying layer. Therefore, neither capillary rise nor water contents exceeding field capacity can be simulated. However, many authors (e.g., Stöckle et al., 1997; Confalonieri et al., 2010c) have demonstrated the reliability of this approach when compared to more sophisticated models based, e.g., on numerical solutions (e.g., van Dam and Feddes, 2000) of the Richards equation (Richards, 1931), especially in cases when there is limited availability (or total unavailability) of spatially distributed information of physical soil properties like, e.g., saturated hydraulic conductivity. In these cases, indeed, the generation of missing inputs – like, e.g., saturated hydraulic conductivity – using pedotrasfer functions (e.g., van Genuchten, 1980) could lead to uncertainty that propagates in an unpredictable way along the modelling chain. The goodness of the cascading approach is demonstrated by the fact that it is adopted by many popular crop models, such as CERES (Ritchie and Otter, 1985), EPIC (Williams et al., 1989), WOFOST (van Keulen et al., 1986), and CropSyst (Stockle et al., 1997).

Root water uptake was simulated using an approach derived from the CERES model (Ritchie and Otter, 1985), based on two steps for estimating actual water uptake (potential one is estimated based on maximum evapotranspiration):

1. for each soil layer, the soil water content is compared with the root water requests (which in turn depends on potential transpiration);
2. if the root water request cannot be completely satisfied for one or more soil layers, it is possible to use a compensation function to move part of the root water request towards soil layers with more water available. After considering the compensation, the total root water request is reduced according to the water availability in the soil layers.

Water requests for the different soil layers are estimated based on root length density, the latter estimated according to the van den Berg-Driessen model (van den Berg and Driessen, 2002). The Campbell's (Campbell, 1974) soil water retention function is used to account for the relationship between volumetric soil water content and matrix suction, to reproduce the effect of the decrease in soil water potential on the plant capability to uptake water.

Simulations were run for five ideal cultivars differing for the thermal time needs: early, medium-early, medium, medium late, late.
To properly account for inter-annual variability in weather conditions, simulations were run for the seasons from 2009 to 2020.

Results and discussion

Results from the simulations of crop (maximum) and actual evapotranspiration allowed deriving the water deficit for each of the simulation units deriving from overlapping weather and soil data layers. Spatially distributed simulation outputs (water deficit maps) were then used to analyze the spatial and temporal variability in water deficit values for each of the five groups of cultivars (section "*Water deficit maps*" in this document). The analysis of spatial and temporal dynamics, as well as information on land use (vineyards distribution from CORINE Land Cover v. 2018; CLC2018; Briggs and Mounsey, 1989; Aune-Lundberg and Strand, 2021) and the knowledge of the study areas, supported the identification of the DEMO farms, for which seasonal dynamics of crop (maximum) and actual evapotranspiration were analized (section "*Identification of the DEMO farms*" in this document).

Water deficit maps

Water deficit maps derive from the difference between the unlimited evapotranspiration of vineyards (ETc) and the actual one (water limited; ETact), the former being derived from the reference evapotranspiration (ET0) multiplied by a dynamic ET crop coefficient (Kc). Data from a sample season (2019) are shown in Fig. 4, with ET0 in the top map, ETc in the left map, and ETact in the right map.

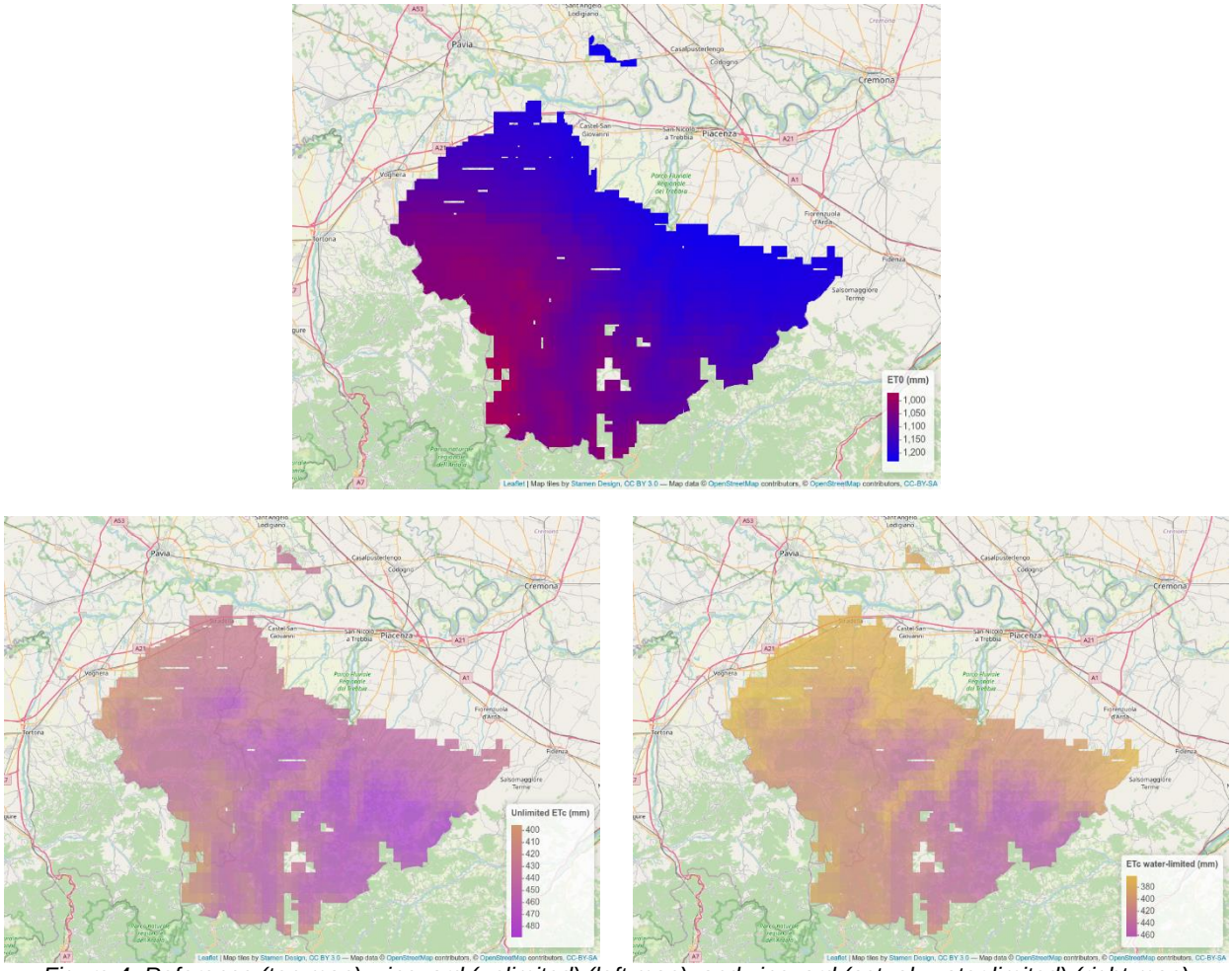

Figure 4. Reference (top map), vineyard (unlimited) (left map), and vineyard (actual, water limited) (right map) evapotranspiration for the study area. These sample maps refer to the 2019 season.

Despite differences in the spatial patterns and in the extent of the mean seasonal water deficit simulated for the five groups of cultivars (Figs. 5, 7, 9, 11 and 13), a general tendency can be observed, with larger deficits estimated for the eastern part of the study area. However, high water deficit values can be observed also in the norther municipalities while moving to the groups of cultivars with higher thermal requirements. This is particularly clear especially for medium late (Fig. 11) and late (Fig. 13) cultivars, although also early medium (Fig. 7) and medium (Fig. 9) ones – although to a lesser extent – present a similar tendency.

Concerning the interannual variability in the seasonal water deficit (Figs. 5, 7, 9, 11 and 13), the northern part of the study area results as the one characterized by the highest heterogeneity among years. This means that farms that are located in the northern municipalities present the largest seasonal effect on water deficit. This is particularly true for the early (Fig. 5) and medium-early (Fig. 7) groups of cultivars. The overall lower extent of the variability in water deficit among years for medium-late (Fig. 11) and late (Fig. 13) cultivars is likely due to the fact that shorter crop cycles expose plants to a higher risk of unfavourable conditions for rain, whereas longer cycles can be characterized by a higher probability that wet periods compensate dry ones during the season.

Concerning the variability among years (from 2009 to 2020) (Figs. 6, 8, 10, 12 and 14), 2009, 2010, 2011, and 2014 present the lowest water deficit values, regardless of the thermal requirements of the group of cultivar considered. The highest deficit values are instead simulated for 2012, 2013, 2020 and – to a lower extent – for 2018. For these years, the water deficit increases with the thermal requirements of the different groups of cultivars, with an overall increasing trend while moving from early cultivars (Fig. 6) to late ones (Fig. 14). Years 2016, 2018 and 2019 are instead characterized by an intermediate water deficit and with a pattern while moving from early to late cultivars similar to the one observed for 2012, 2013, 2018 and 2020. However, spatial patterns are different among the three years, with 2016 and 2018 presenting

the largest deficit values in the eastern part of the study area, whereas 2019 is characterized by the largest water deficit values in the northern municipalities.

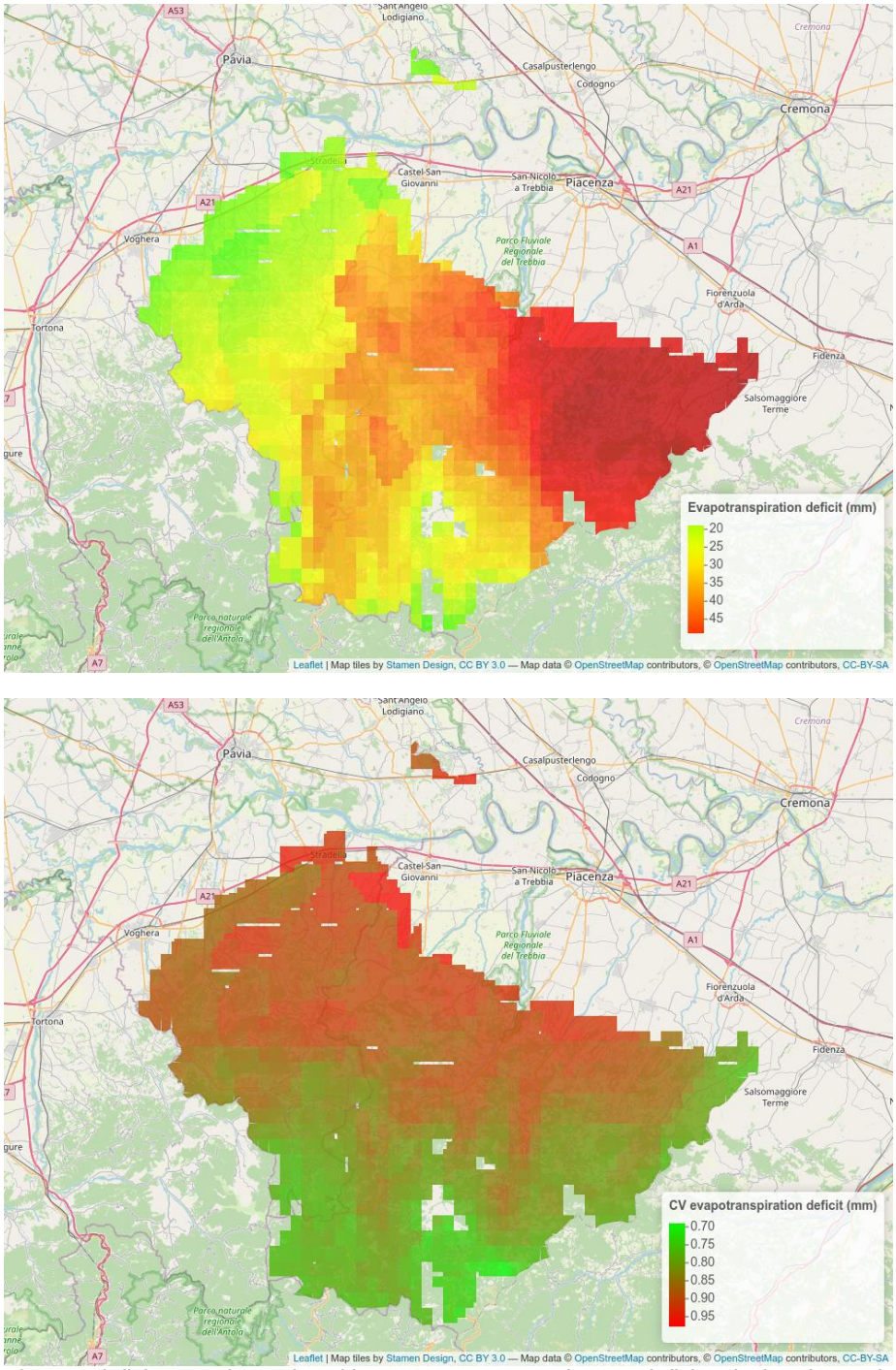

Figure 5. Seasonal water deficit maps for early cultivars. Mean seasonal water deficit calculated over the 2009-2020 time frame is shown in the top map; related coefficient of variation calculated among the seasonal water deficits is shown in the bottom map.

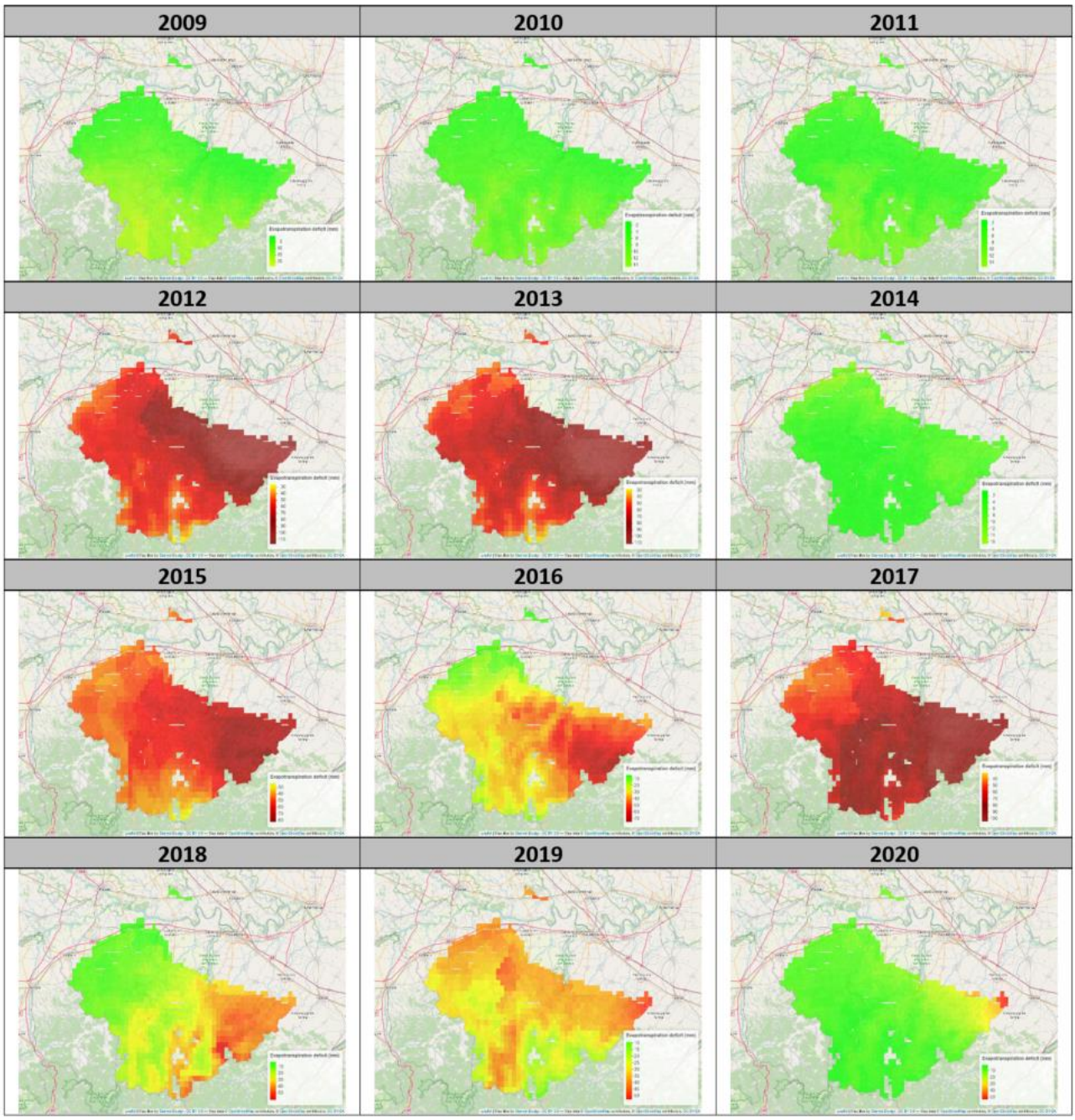

Figure 6. Seasonal water deficit maps for early cultivars from 2009 to 2020.

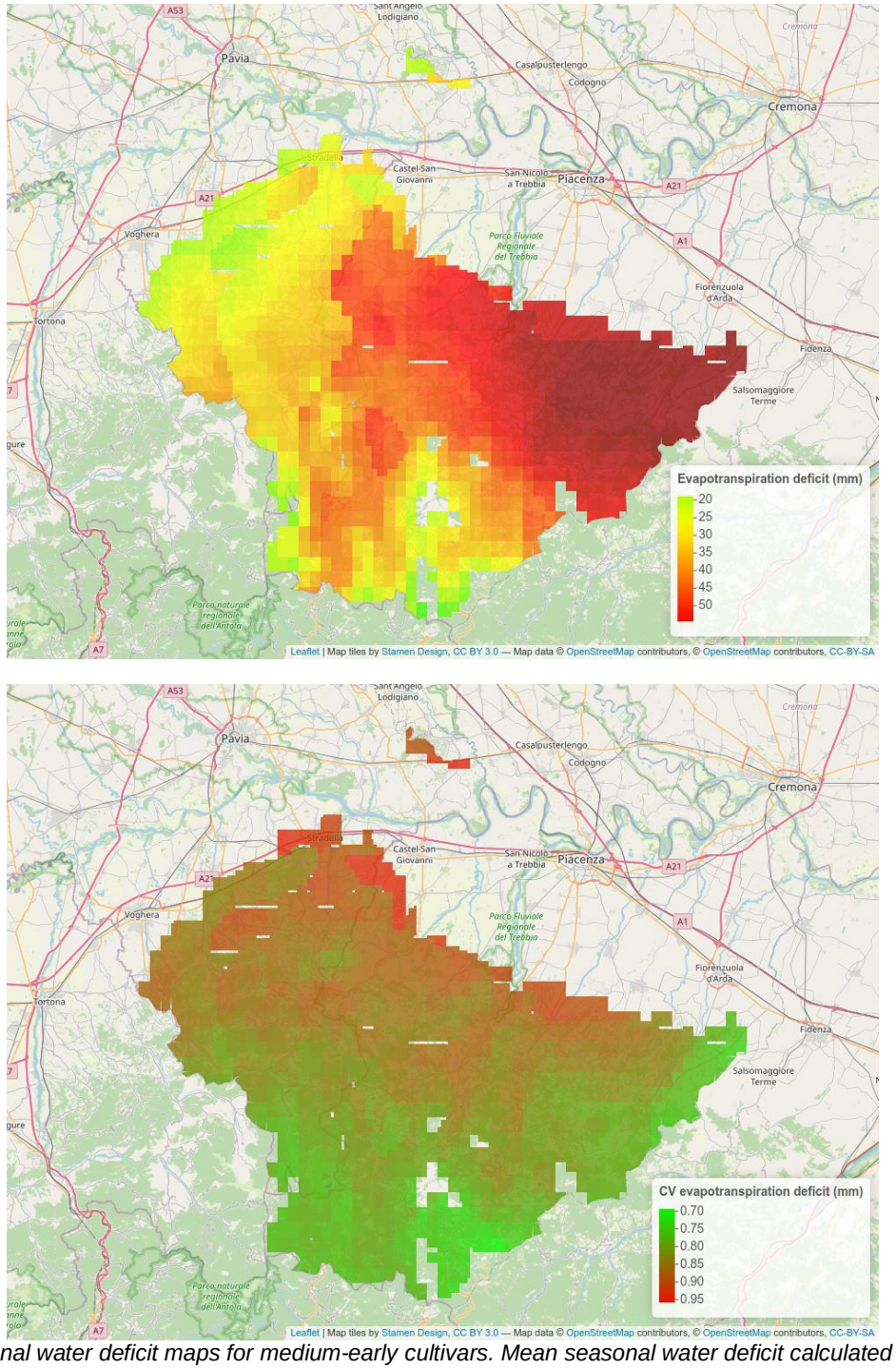

Figure 7. Seasonal water deficit maps for medium-early cultivars. Mean seasonal water deficit calculated over the 2009-2020 time frame is shown in the top map; related coefficient of variation calculated among the seasonal water deficits is shown in the bottom map.

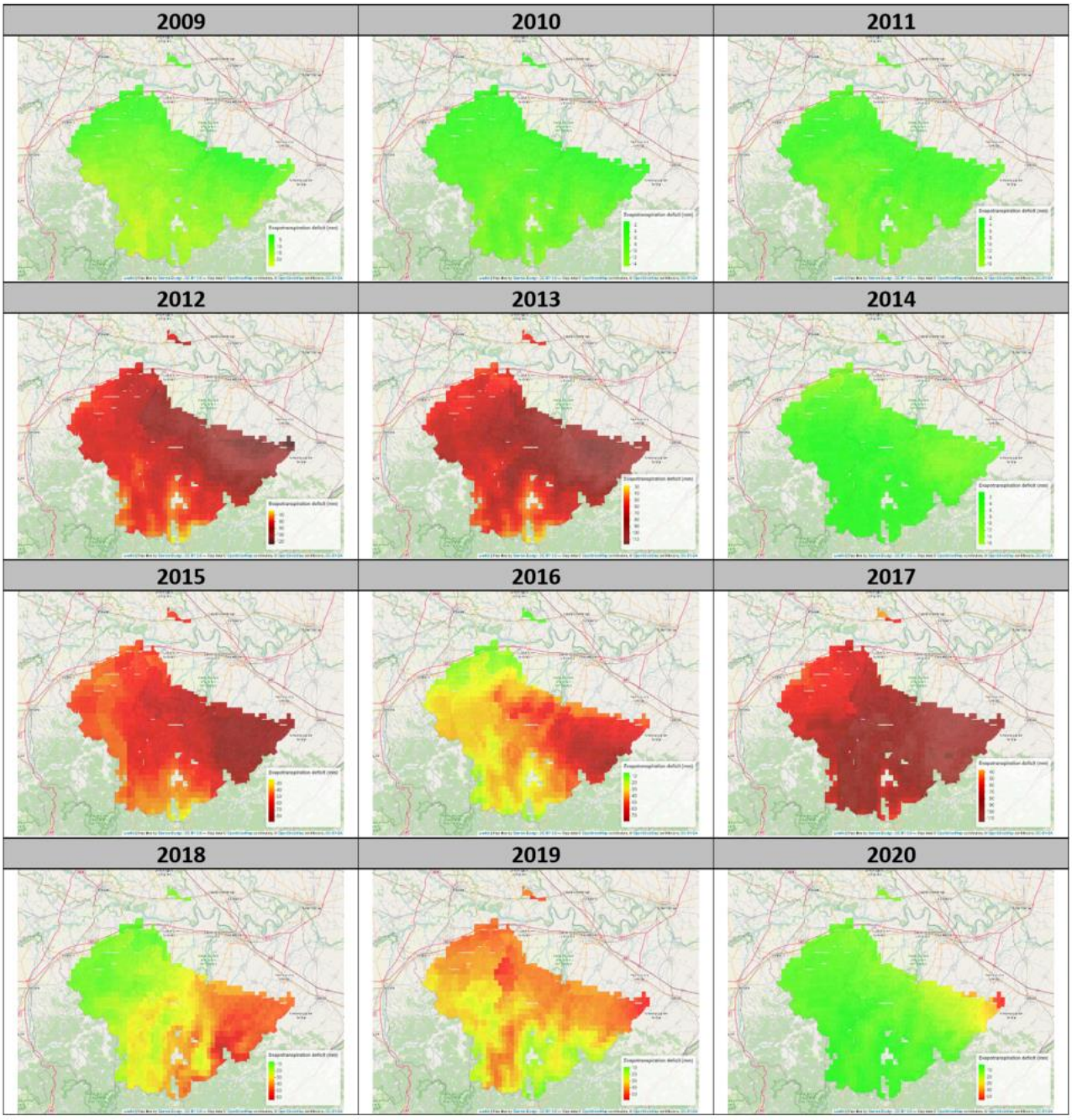

Figure 8. Seasonal water deficit maps for medium-early cultivars from 2009 to 2020.

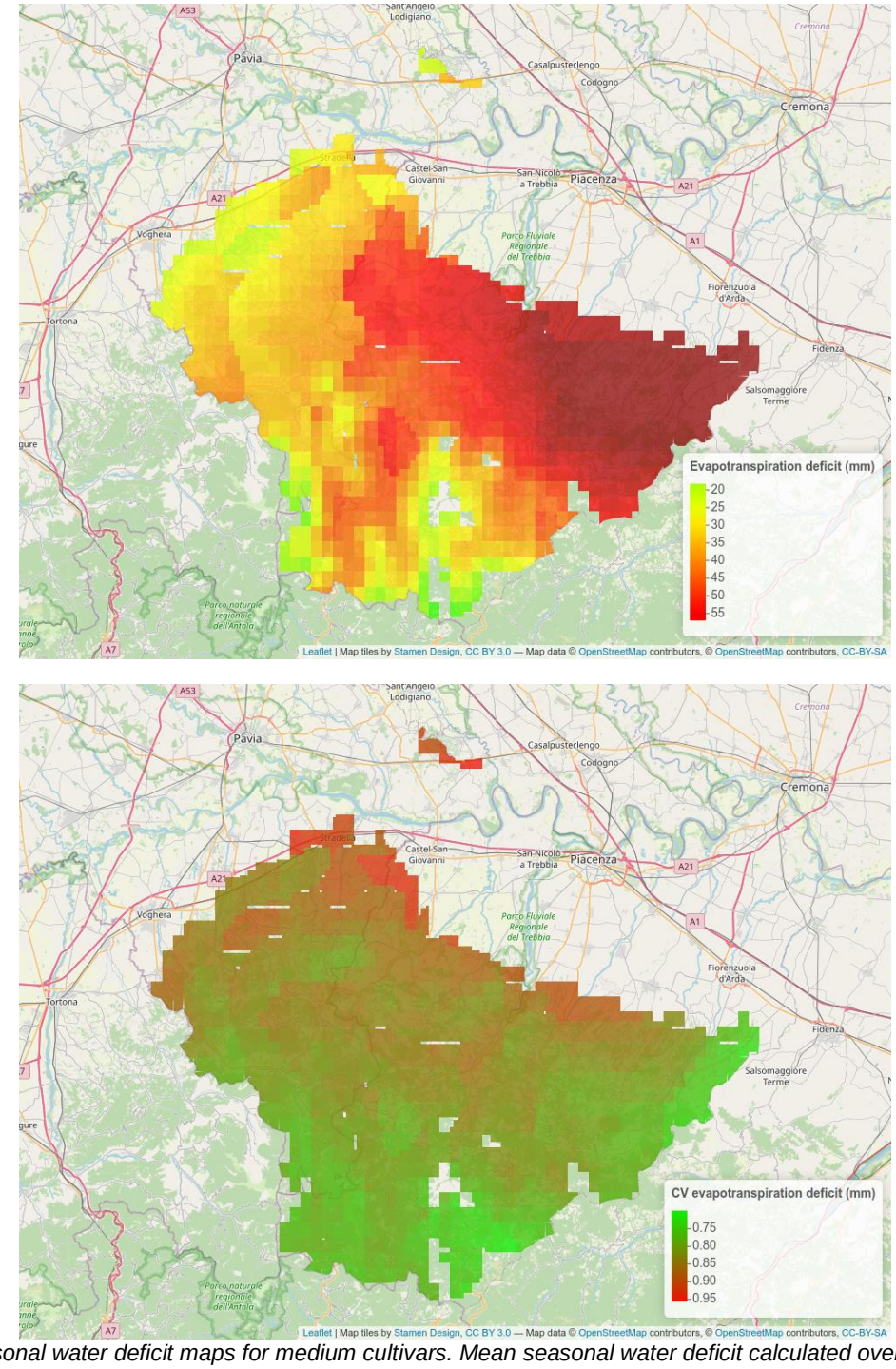

Figure 9. Seasonal water deficit maps for medium cultivars. Mean seasonal water deficit calculated over the 2009-2020 time frame is shown in the top map; related coefficient of variation calculated among the seasonal water deficits is shown in the bottom map.

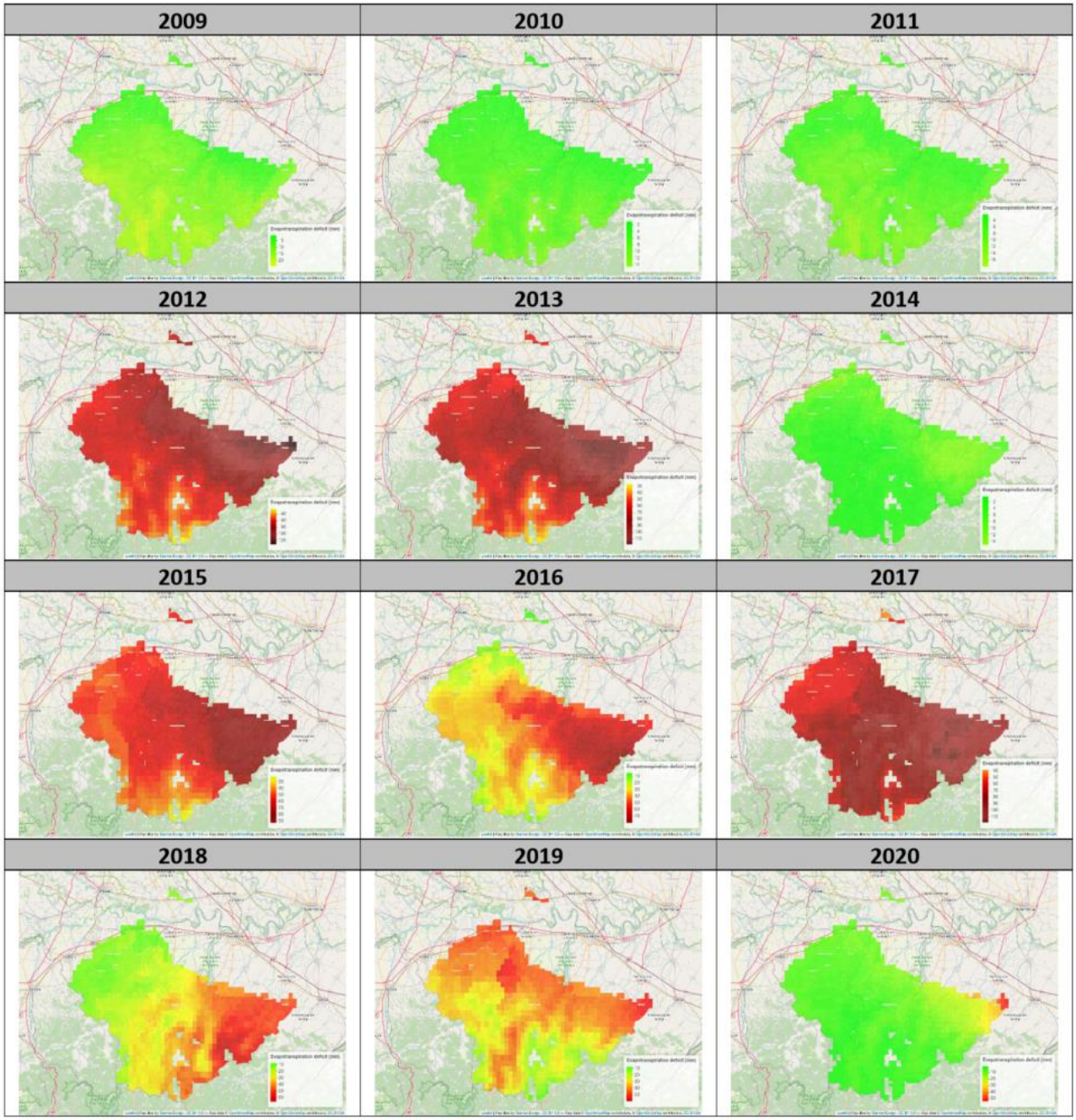

Figure 10. Seasonal water deficit maps for medium cultivars from 2009 to 2020.

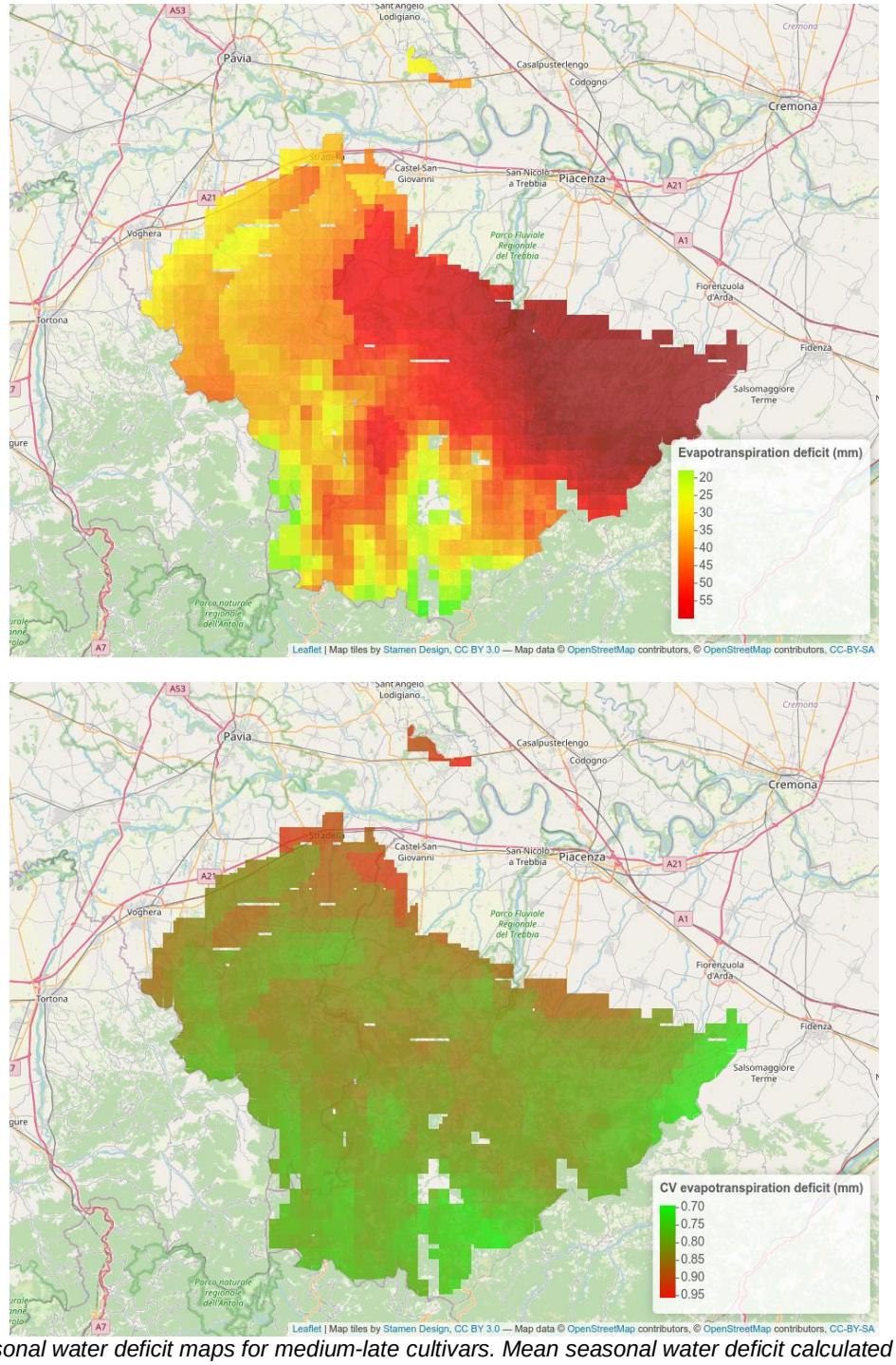

Figure 11. Seasonal water deficit maps for medium-late cultivars. Mean seasonal water deficit calculated over the 2009-2020 time frame is shown in the top map; related coefficient of variation calculated among the seasonal water deficits is shown in the bottom map.

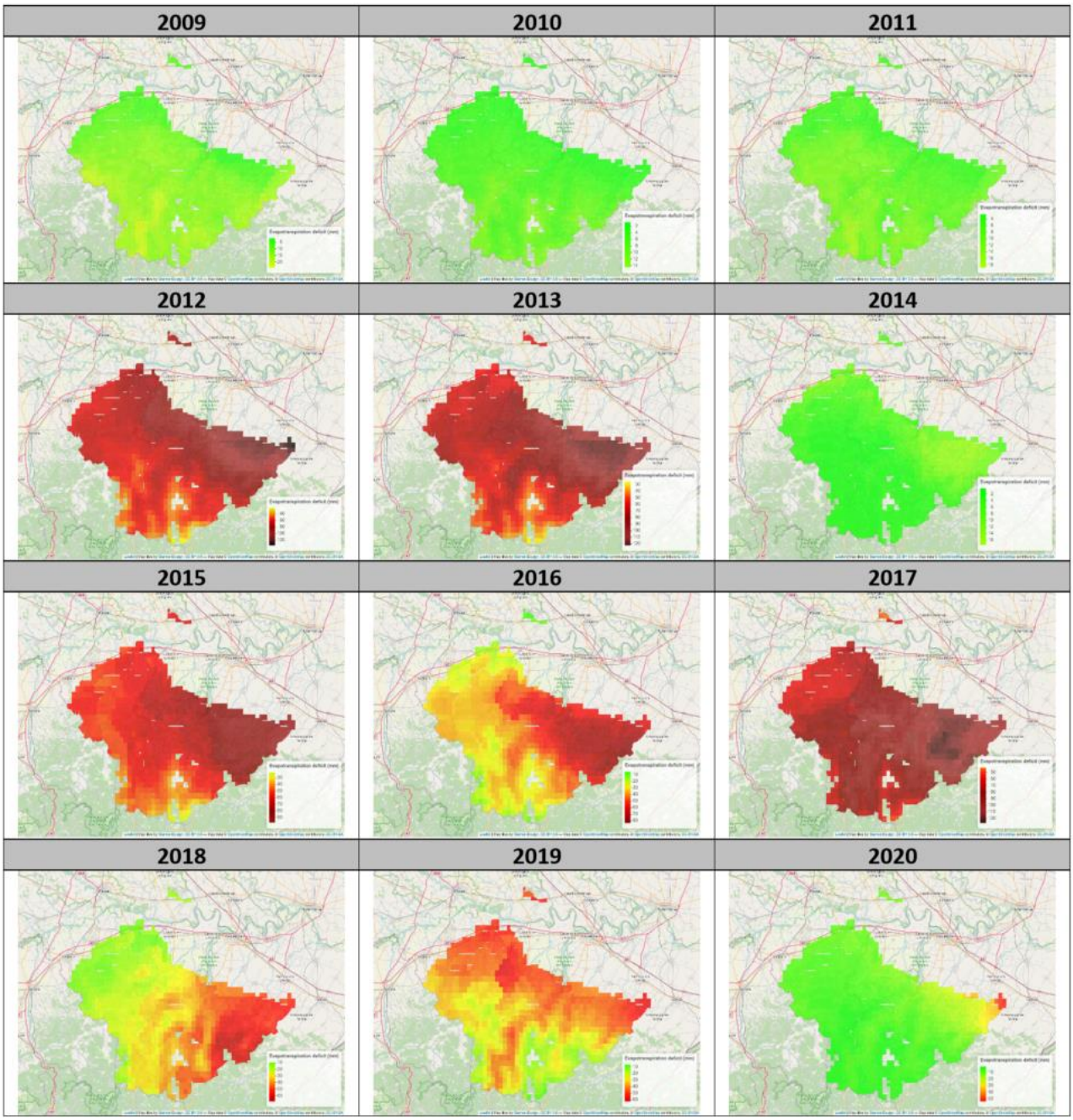

Figure 12. Seasonal water deficit maps for medium-late cultivars from 2009 to 2020.

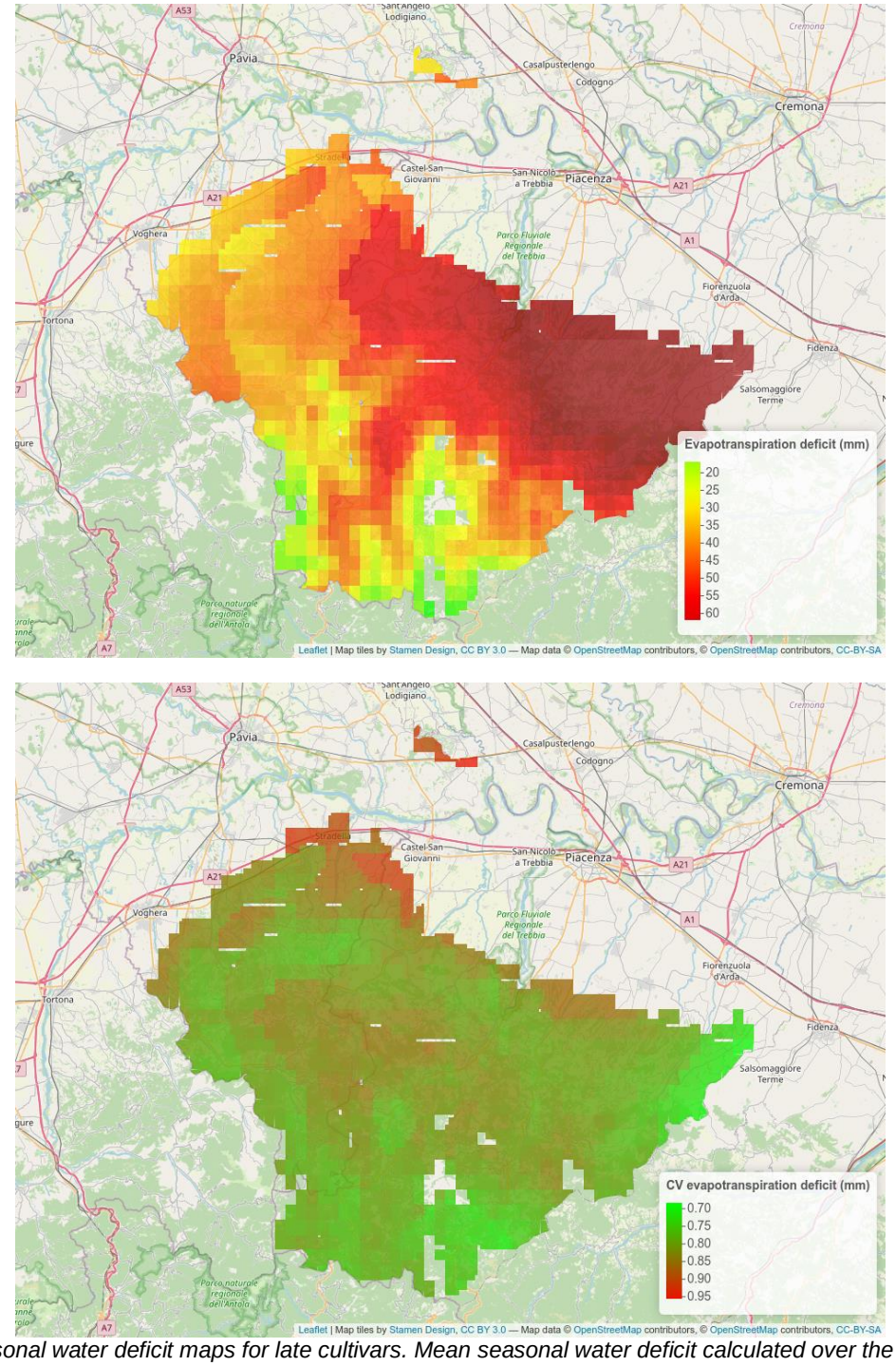

Figure 13. Seasonal water deficit maps for late cultivars. Mean seasonal water deficit calculated over the 2009-2020 time frame is shown in the top map; related coefficient of variation calculated among the seasonal water deficits is shown in the bottom map.

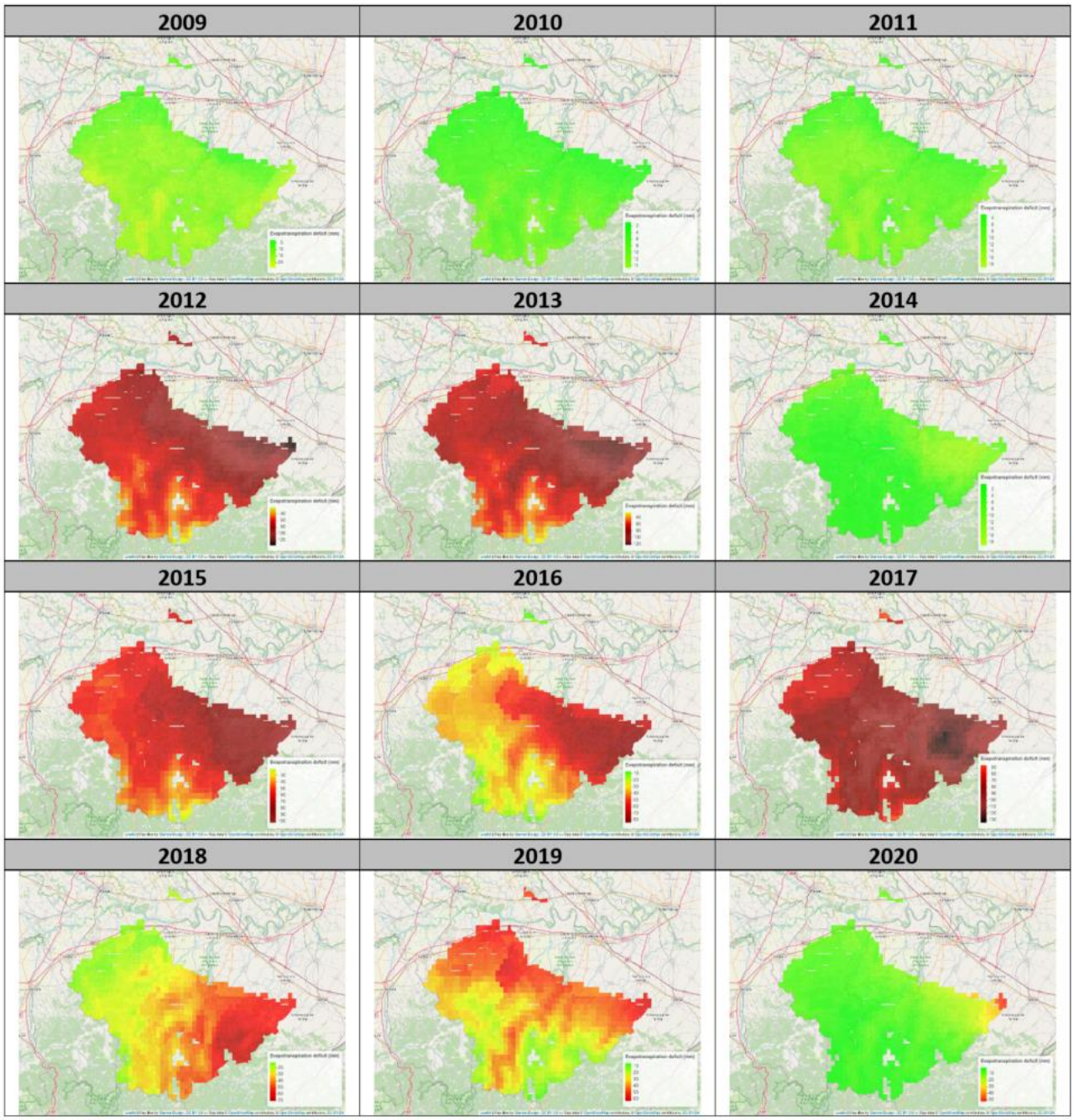

Figure 14. Seasonal water deficit maps for late cultivars from 2009 to 2020.

Identification of the DEMO farms

Mapping water deficit (see section "*Water deficit maps*" in this document) allowed analyzing spatial and temporal patterns of water deficit in the study area. In particular, mean seasonal water deficit maps calculated over the 2009-2020 time frame (Figs. 5, 7, 9, 11 and 13) underlined how the eastern and – to a lesser extent – northern parts of the study area are generally the most exposed to conditions characterized by insufficient water availability, with the northern part (where the density of vineyards per unit soil surface is the highest according to CORINE Land Cover vineyard class) exposed to the largest inter-annual variability in water stress.

Based on these considerations, the analysis of water deficit maps allowed defining the following criteria to identify the part of the study area where the DEMO farms should be located:

- presence of medium or medium-high mean water deficit;
- high inter-annual variability in water deficit;
- high concentration of vineyards from land use maps.

These criteria led to identify the northern part of the study area as the most suitable to perform the experiments related with the other project activities. The identified DEMO farms are shown in Fig. 14 and presented – together with key physical soil properties – in Table 2.

This analysis and the derived choice of the DEMO farms will allow facing the water deficit issues in an effective way during the other project activities.

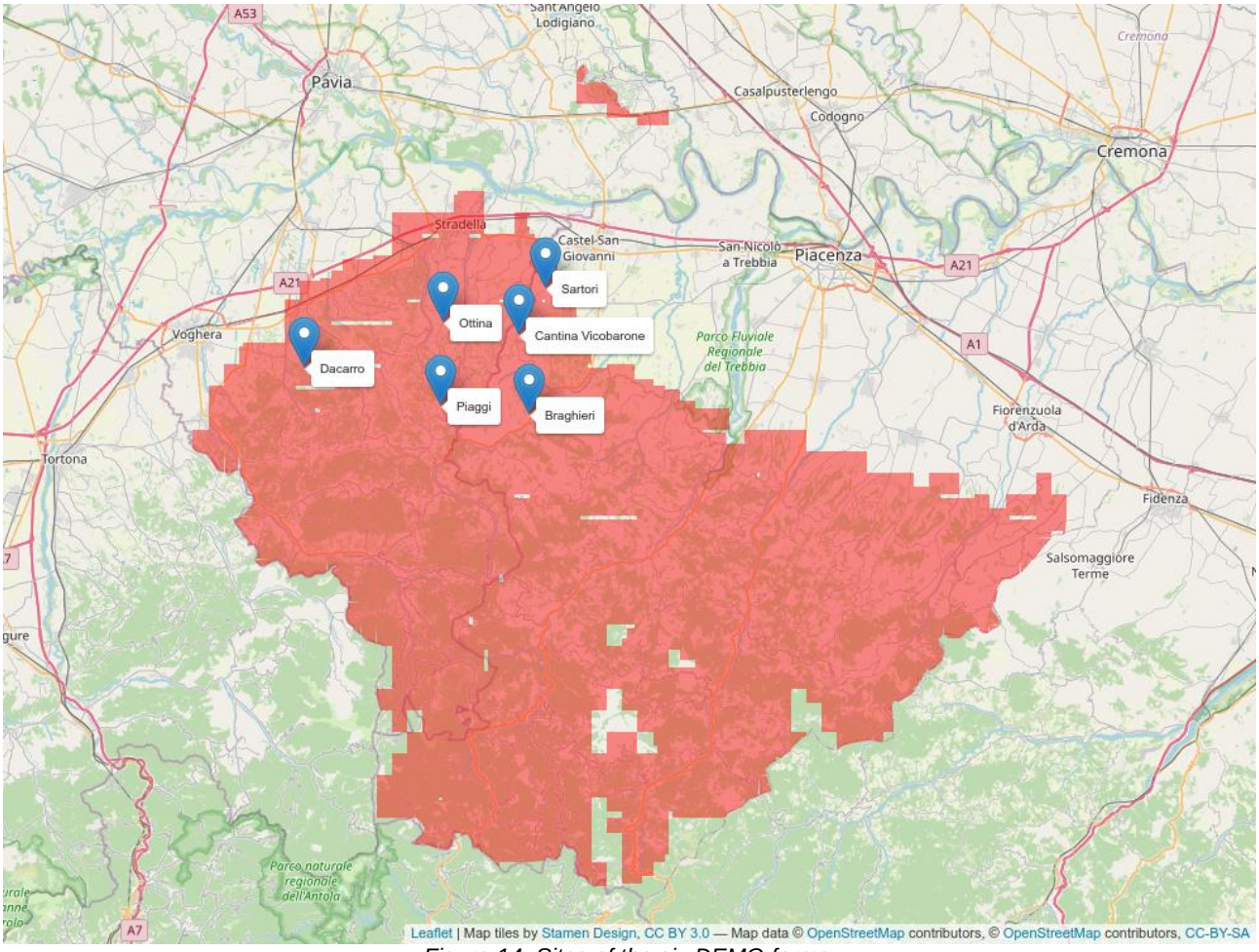

Figure 14. Sites of the six DEMO farms.

Table 2. The six DEMO farms identified based on the water deficit maps.

Farm name	Latitude (° N)	Longitude (° E)
Braghieri	44.90	9.37
Cantina Vicobarone	44.99	9.36
Sartori	45.03	9.39
Dacarro	44.97	9.12
Ottina	45.00	9.28
Piaggi	44.94	9.27

Mean (calculated over the 2009-2020 time frame) seasonal dynamics of maximum ("Crop" according to the FAO terminology) and actual evapotranspirations for the six DEMO farms are shown in Figs. from 15 to 17, together with related standard deviations quantifying the inter-annual variability. The difference between the two evapotranspiration represents the water deficit. Data are presented for the five groups of cultivars differing for their thermal requirements. Besides the mean values for the two evapotranspirations that are discussed below based on the diagram shown in Fig. 18, Figs. 15 to 17 highlight the great inter-annual variability, especially in the case of actual evapotranspiration.

In general, light water deficit starts around 15 June for early cultivars (Fig. 18), with earliest water deficits simulated for the DEMO farms Sartori, Dacarro and Cantina Vicobarone, and the latest deficits simulated for Piaggi and Ottina. For the same group of cultivars, light deficits end at the beginning of September, with few differences among the six DEMO farms. Relevant water deficits for the same cultivats are simulated from 20 July to 15/20 August for all DEMO farms but Braghieri, for which the duration of the relevant water deficit period ends at the end of August.

Light and relevant water deficits for medium-early cultivars start consistently with what discussed for early ones, but ends up two weeks later for the the DEMO farms Braghieri and Piaggi in the case of light deficit and about one week later for the relavant deficit (Fig. 18).

The starting periods for light and relevant water deficits in the case medium cultivars are practically overlapped with those simulated for medium-early ones (Fig. 18), the only exception being the DEMO farm Dacarro, for which a 2-week delay was simulated for the light deficit. A great consistency between simulated water deficits for medium and early-medium cultivars was observed also for the ending periods, although in this case less than a 1-week delay was estimated for medium-early cultivars. Only exceptions are the DEMO farms Piaggi, Ottina and Sartori, for which the delay was almost two weeks.

The situation for medium-late and late cultivars was very similar to that discussed for medium ones (Fig. 18). The only exceptions were the medium-late cultivars in the DEMO farm Cantina Vicobarone, for which the light water deficit starts with a 10-day delay when moving both from medium to medium-late and from medium-late to late cultivars, and the late cultivars in the DEMO farm Piaggi, for which the relevant water deficit ends up to 10 days later compared to what simulated for medium and medium-late cultivars.

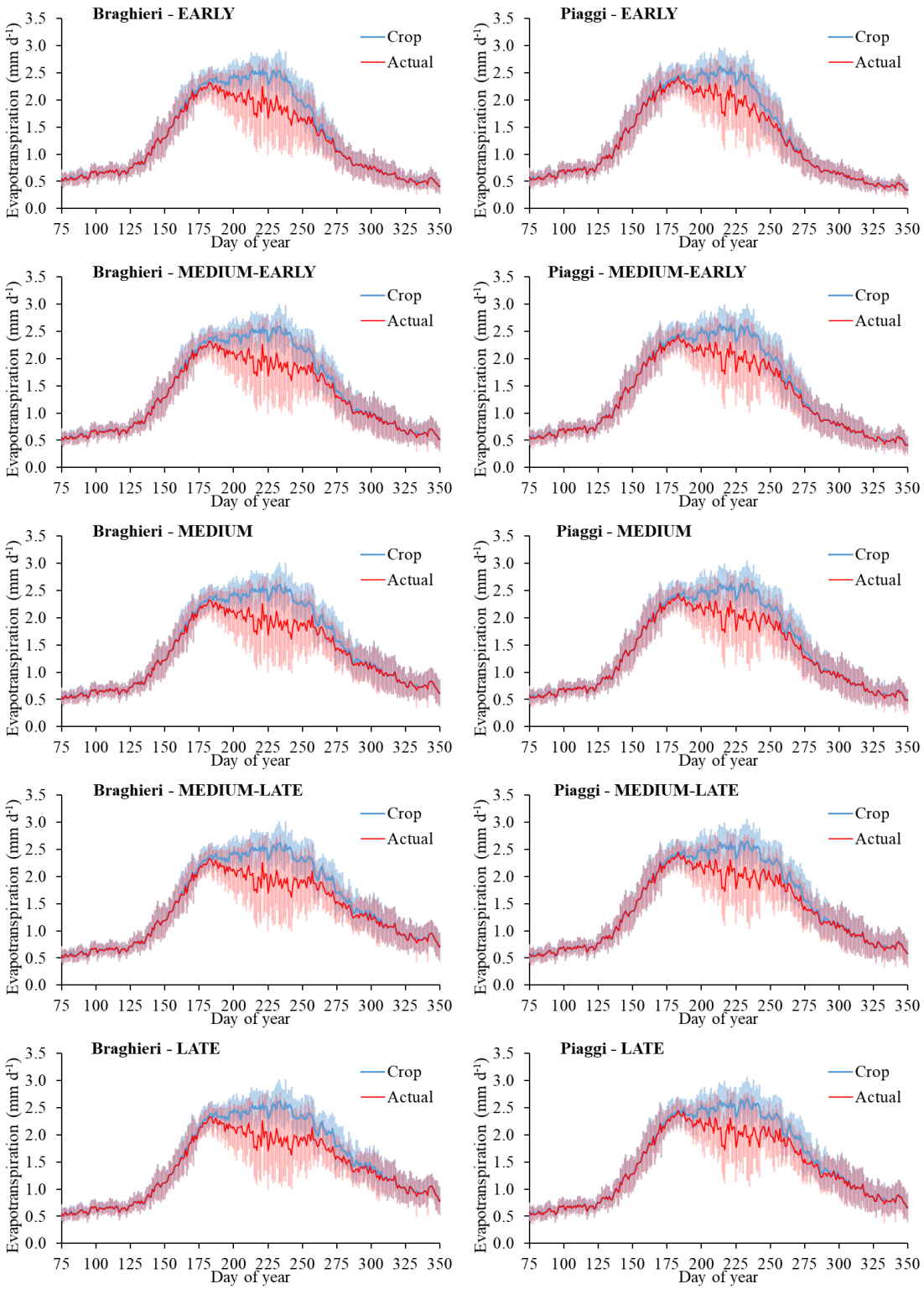

Figure 15. Seasonal dynamics of crop (maximum) and actual evapotranspiration, the difference between the two series representing the water deficit. Solid lines represent mean values calculated over the period 2009-2020; the buffers indicate the related standard deviations. Dynamics for five groups of cultivars differing for thermal requirements (early, medium-early, medium, medium-late, and late) are shown. Data for the Braghieri DEMO farm are shown on the left charts, data for the Piaggi DEMO farm are in the right charts.

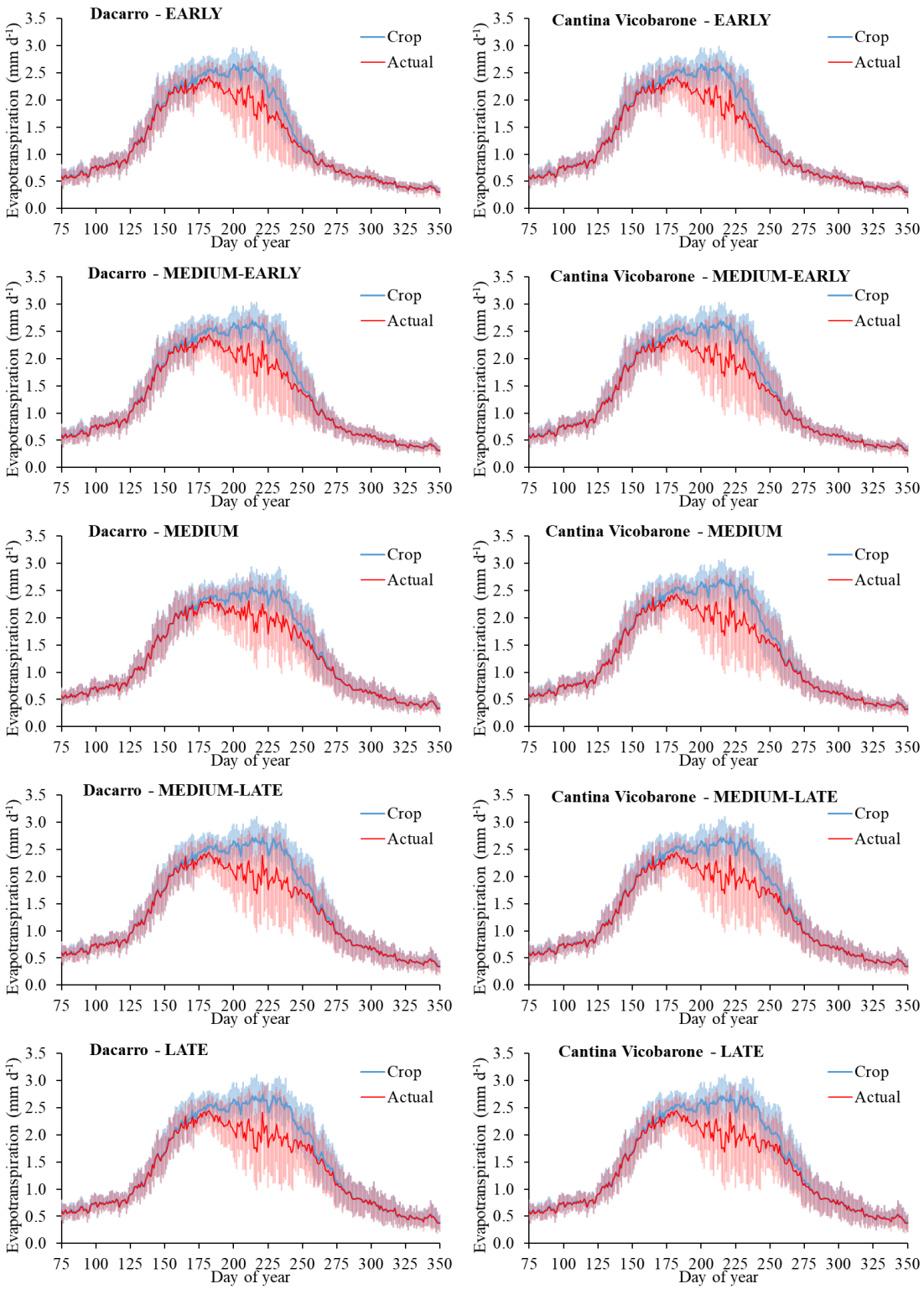

Figure 16. Seasonal dynamics of crop (maximum) and actual evapotranspiration, the difference between the two series representing the water deficit. Solid lines represent mean values calculated over the period 2009-2020; the buffers indicate the related standard deviations. Dynamics for five groups of cultivars differing for thermal requirements (early, medium-early, medium, medium-late, and late) are shown. Data for the Dacarro DEMO farm are shown on the left charts, data for the Cantina Vicobarone DEMO farm are in the right charts.

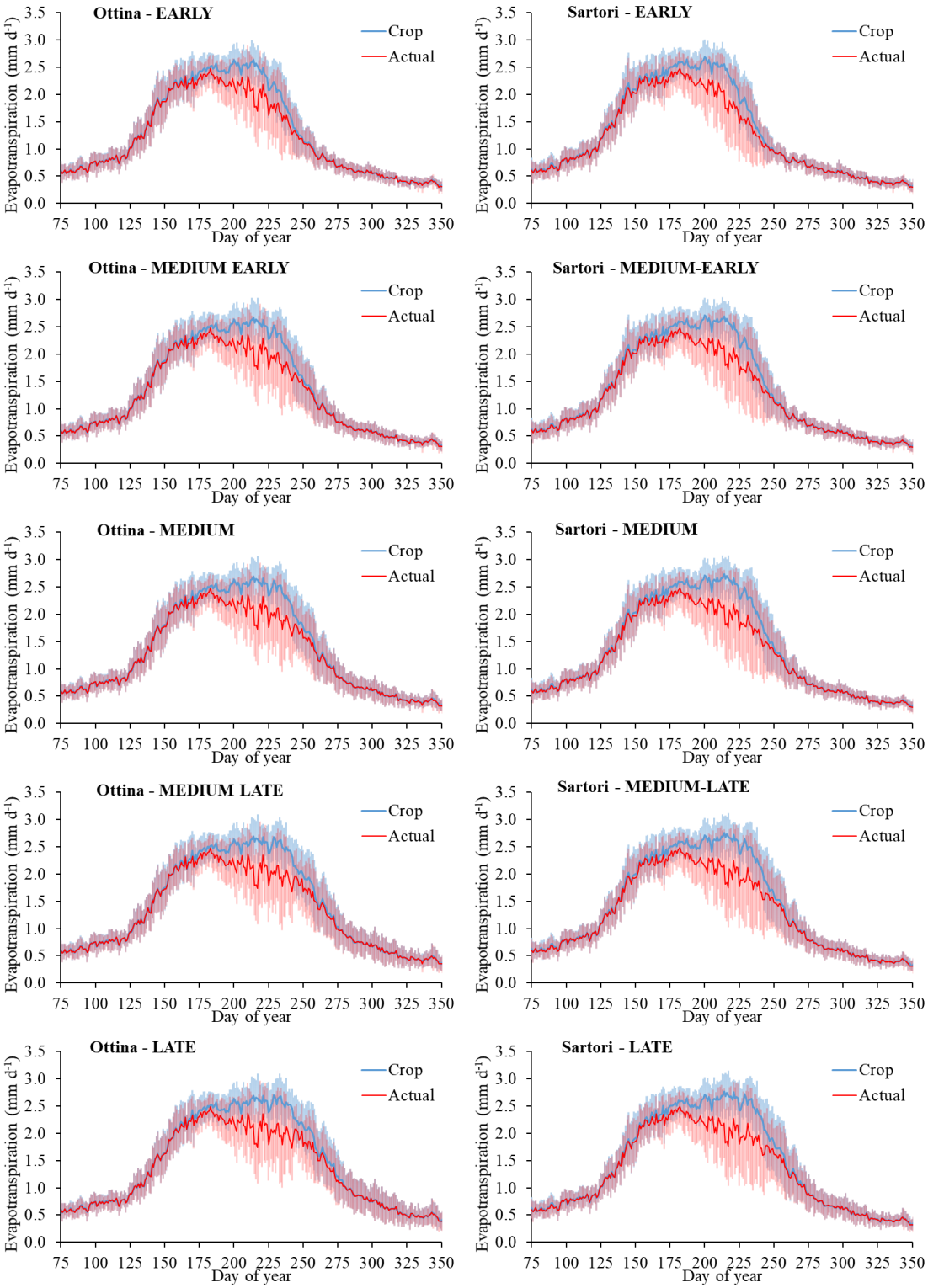

Figure 17. Seasonal dynamics of crop (maximum) and actual evapotranspiration, the difference between the two series representing the water deficit. Solid lines represent mean values calculated over the period 2009-2020; the buffers indicate the related standard deviations. Dynamics for five groups of cultivars differing for thermal requirements (early, medium-early, medium, medium-late, and late) are shown. Data for the Ottina DEMO farm are shown on the left charts, data for the Sartori DEMO farm are in the right charts.

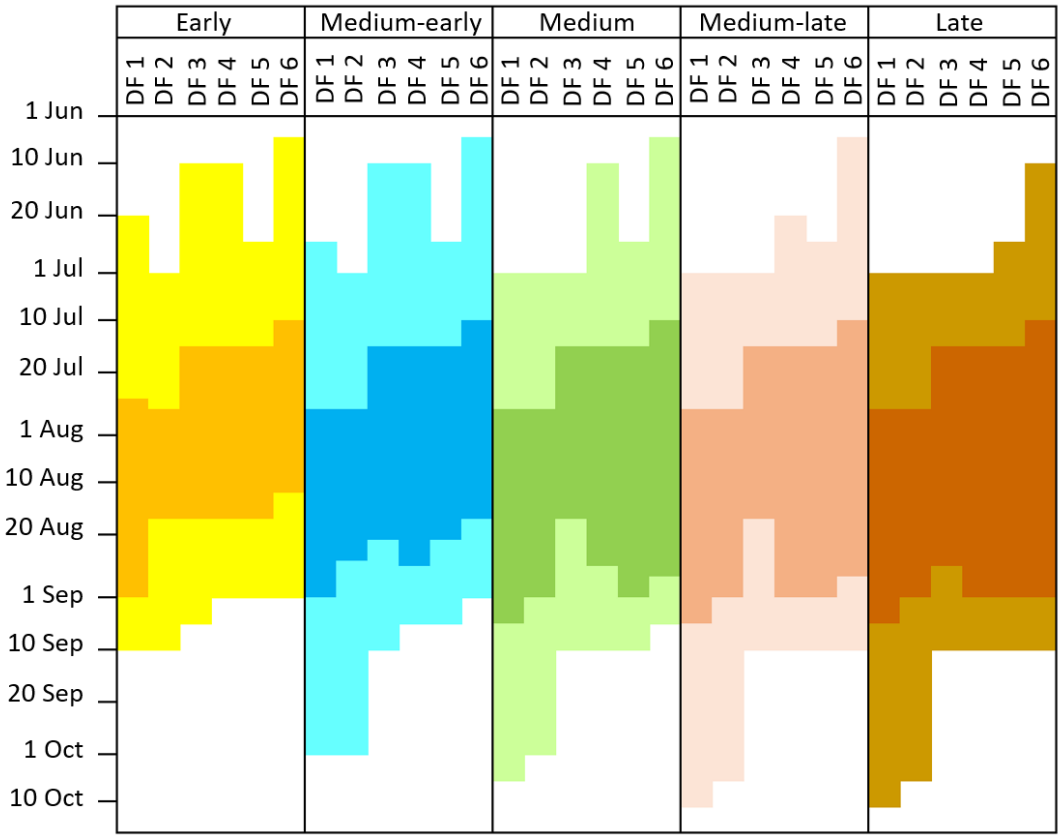

Figure 18. Duration of the water deficit periods for the five groups of cultivars (differing for length of the cycle) in the six DEMO farms. DF 1, DF 2, DF 3, DF 4, DF 5, DF 6 refer to DEMO farms Braghieri, Piaggi, Dacarro, Cantina Vicobarone, Ottina, Sartori, respectively (Table 2). Light colors refer to light water deficits, dark colors to relevant water deficits.

References

Allen, R.G., Pereira, L.S., Raes, D., Smith, M., 1998. Crop evapotranspiration: guidelines for computing crop water requirements, Irrigation and Drainage Paper 56. United Nations FAO, Rome, 300 p.

Aune-Lundberg, L., Strand, G.-H., 2021. The content and accuracy of the CORINE Land Cover dataset for Norwey. International Journal of Applied Earth Observation and Geoinformation, 96, 102266.

Batjes, N.H., 2016. Harmonized soil property values for brouad-scale modelling (WISE30sec) with estimates of global soil carbon stocks. Geoderma, 269, 61-68.

Briggs, D., Mounsey, H., 1989. Integrating land resource data into a European geographical information system: practicalities and problems. Applied Geography, 9, 5-20.

Budyko, M.I., 1974. Climate and life. Academic Press, New York, USA.

Calò, A., Costacurta, A., Tomasi, D., Biscaro, S., 1997. La fenologia della vite in Italia in rapporto alle condizioni ambientali. In Calò A. (ed): Il determinismo climatico sulla fenologia della vite e la maturazione dell'uva in Italia. Arti grafiche. Conegliano (TV), 14-15 luglio 93, p. 3-71.

Campbell, G.S., 1974. A simple method for determining unsaturated conductivity from moisture release data. Soil Science, 117, 311-314.

Carter, D.B., Mather, R., 1966. Climatic classification for environmental biology. C.W. Thornwaite Association, Publications in Climatology, 19, 305-395.

Cola, G., Failla, O., Maghradze, D., Megrelidze, L., Mariani, L., 2017. Grapevine phenology and climate change in Georgia. International Journal of Biometeorology, 61, 761-773.

Cola, G., Mariani, L., Maghradze, D., Failla, O., 2020. Changes in thermal resources and limitations for Georgian viticulture. Australian Journal of Grape and Wine Research, 26, 29-40.

Cola, G., Mariani, L., Salinari, F., Civardi, S., Bernizzoni, F., Gatti, M., Poni, S., 2014. Description and testing of a weather-based model for predicting phenology, canopy development and source-sink balance in *Vitis vinifera* L. cv. Barbera. Agricultural and Forest Meteorology, 184, 117-136.

Confalonieri, R., Bellocchi, G., Donatelli, M., 2010a. A software component to compute agro-meteorological indicators. Environmental Modelling & Software, 25, 1485-1486.

Confalonieri, R., Bregaglio, S., Acutis, M., 2010b. A proposal of an indicator for quantifying model robustness based on the relationship between variability of errors and of explored conditions. Ecological Modelling, 221, 960-964.

Confalonieri, R., Bregaglio, S., Bocchi, S., Acutis, M., 2010c. An integrated procedure to evaluate hydrological models. Hydrological Processes, 24, 2762-2770.

De Martonne, E., 1942. Nouvelle carte mondiale de l'indice d'aridité. Annales de Géographie 51, 242-250.

Mariani, M., Alilla, R., Cola, G., Dal Monte, G., Epifani, C., Puppi, G., Failla, O., 2013. IPHEN-a real-time network for phenological monitoring and modelling in Italy. International Journal of Biometeorology, 57, 881-893.

Mariani, L., Cola, G., Bulgari, R., Ferrante, A., Martinetti, L., 2016. Space and time variability of heating requirements for greenhouse tomato production in the Euro-Mediterranean area. Science of the Total Environment, 562, 834-844.

Mariani, L., Parisi, S.G., Cola, G., Failla, O., 2012. Climate change in Europe and effects on thermal resources for crops. International Journal of Biometeorology, 56, 1123-1134.

Meier, U., 2003. Phenological growth stages. In: Schwartz M.D. (ed.), Phenology: AnIntegrative Science. Kluver Academic, The Netherlands, pp. 269-283.

NOAA, 2020a. https://data.noaa.gov/dataset/dataset/global-surface-summary-of-the-day-gsod/

NOAA, 2020b. https://tgftp.nws.noaa.gov/data/observations/metar/stations/

NOAA, 2020c. https://tgftp.nws.noaa.gov/SL.us008001/DF.an/DC.sflnd/DS.synop/

NOAA, 2020d. https://www.emc.ncep.noaa.gov/emc/pages/numerical_forecast_systems/gfs.php

Richards, L.A., 1931. Capillary conduction of liquids thrugh porous medium. Physics, 1, 318-333.

Riou, C., Valancogne, C., Pieri, P., 1989. Un modele simple d'interception du rayon-nement solaire par la vigne. Vérification expérimentale. Agronomie, 9, 441-450.

Ritchie, J.T., Otter, S. 1985. Description and performance of CERES-Wheat: A user- oriented wheat yield model. In W.O. Willis (ed.). ARS Wheat Yield Project. U.S. Dept. of Agriculture, Agricultural Research Service. ARS-38. Washington, DC., pp. 159-175.

Romano, N., Brunone, B., Santini, A. 1998. Numerical analysis of one-dimensional unsaturated flow in layered soils. Advances in Water Resources, 21, 315-324.

Stöckle, C.O., Martin, S., Campbell, G.S. 1994. CropSyst, a cropping systems model: water/nitrogen budgets and crop yield. Agricultural Systems, 46, 335-359.

USGS, 2020. https://webgis.wr.usgs.gov/globalgis/gtopo30/gtopo30.htm

van Dam, J.C., Feddes, R.A., 2000. Numerical simulation of infiltration, evaporation and shallow groundwater levels with Richards equation. Journal of Hydrology, 233, 72-85.

van den Berg, M., Driessen, P.M., 2002. Water uptake in crop growth models for land use systems analysis I. A review of approaches and their pedigrees. Agriculture, Ecosystems & Environment, 92, 21-36.

van Genuchten, M.T., 1980. A closed-form equation for predicting the hydraulic conductivity of unsaturated soil. Soil Sci. Soc. of America Journal, 44, 892-898.

van Keulen, H., Wolf, J., 1986. Modelling of agricultural production: weather soils and crops. In: Simulation Monographs. Pudoc, Wageningen, The Netherlands, p. 479.

Williams, J.R., Jones, C.A., Kiniry, J.R., Spanel, D.A., 1989. The EPIC crop growth model. Transactions of ASAE, 32, 497-511.